Detecting single-electron tunneling involving virtual processes in real time

S. Gustavsson,[*] M. Studer, R. Leturcq, T. Ihn, and K. Ensslin

Solid State Physics Laboratory, ETH Zürich, CH-8093 Zürich, Switzerland

D. C. Driscoll and A. C. Gossard

Department of Materials, University of California–Santa Barbara, Santa Barbara, California 93106, USA

We use time-resolved charge-detection techniques to probe virtual tunneling processes in a double quantum dot. The process involves an energetically forbidden state separated by an energy δ from the Fermi energy in the leads. The nonzero tunneling probability can be interpreted as cotunneling, which occurs as a direct consequence of time-energy uncertainty. For small energy separation the electrons in the quantum dots delocalize and form molecular states. In this regime we establish the experimental equivalence between cotunneling and sequential tunneling into molecular states for electron transport in a double quantum dot. Finally, we investigate inelastic cotunneling processes involving excited states of the quantum dots. Using the time-resolved charge-detection techniques, we are able to extract the shot noise of the current in the cotunneling regime.

PACS number(s): 73.23.Hk, 73.21.La, 73.63.Kv

I. INTRODUCTION

A semiconductor double quantum dot (DQD) is the mesoscopic analog of a diatomic molecule. The energy levels and the interdot coupling energy can be precisely controlled with gate voltages,[1] which allows the DQD to be tuned to a configuration where the electron wave functions hybridize and form molecular states extending over both quantum dots (QDs). The DQD thus provides a tunable two-level system, which has been utilized to perform coherent manipulation of a single charge in semiconductor nanostructures.[2,3]

An alternative approach to molecular states at large detuning is to study electron transport in the DQD in the framework of cotunneling.[4] Cotunneling involves an electron (or hole) that virtually tunnels through an energetically forbidden charge state of the QD positioned at an energy δ away from the Fermi energy in the leads. The process occurs on a timescale $\tau_{\text{cot}} \sim \hbar / \delta$ limited by time-energy uncertainty.[5] Cotunneling currents are generally small and difficult to measure but the effect has been utilized for QD spectroscopy,[6,7] for studying cotunneling-mediated transport in single QDs,[8] or for investigating spin effects in double QDs.[9]

In this work we use a quantum point contact (QPC) as a charge sensor[10] to detect single-electron tunneling in the DQD in real time.[11–13] Similar setups have been used for investigating single-spin dynamics,[14] for detecting single-particle interference,[15] for probing interactions between charge carriers,[16] or for measuring extremely small currents.[17,18] Here, we utilize the technique to count electrons cotunneling through the DQD. The method provides a precise measurement of the tunneling probability as a function of energy separation δ between the QDs, allowing a direct comparison with the rate expected from time-energy uncertainty. In the limit of $\delta \rightarrow 0$, the electrons form molecular states extending over both QDs. Here, we measure tunneling rates expected from sequential tunneling into bonding and antibonding states of the DQD. The results experimentally establish the equivalence between cotunneling into

coupled QD states and sequential tunneling into molecular states of the DQD.

In Sec. VII of the paper we investigate inelastic cotunneling processes involving excited states of the DQD. Finally, we use the time-resolved charge-detection techniques to extract the shot noise of the DQD current in the cotunneling regime.

II. EXPERIMENTAL SETUP AND METHODS

The measurements were performed on the structure shown in Fig. 1(a). The sample is fabricated with local oxidation[19] of a GaAs/Al$_{0.3}$Ga$_{0.7}$As heterostructure containing a two-dimensional electron gas (2DEG) 34 nm below the surface. The structure consists of two QDs (marked by 1 and 2 in the figure) connected by two separate tunnel barriers. Each QD contains about 30 electrons. For the results presented here only the upper tunnel barrier was kept open; the lower was pinched-off by applying appropriate voltages to the surrounding gates. The sample details are described in Ref. 20.

The electron population of the DQD is monitored by operating the QPC in the lower-right corner of Fig. 1(a) as a charge detector.[10] By tuning the tunneling rates of the DQD below the detector bandwidth, charge transitions can be detected in real time.[11–13] In the experiment, the tunneling rates Γ_S and Γ_D corresponding to source and drain leads are kept around 1 kHz, while the interdot coupling t is set much larger ($t \sim 20~\mu$eV ~ 5 GHz). Interdot transitions thus occur on timescales much faster than it is possible to register with the detector ($\tau_{\text{det}} \sim 50~\mu$s),[21] but the coupling energy may still be determined from charge localization measurements.[22] The conductance of the QPC was measured by applying a bias voltage of $200-400~\mu$V and monitoring the current [I_{QPC} in Fig. 1(a)]. We ensured that the QPC bias voltage was kept low enough to avoid charge transitions driven by current fluctuations in the QPC.[20] The sample is realized with-
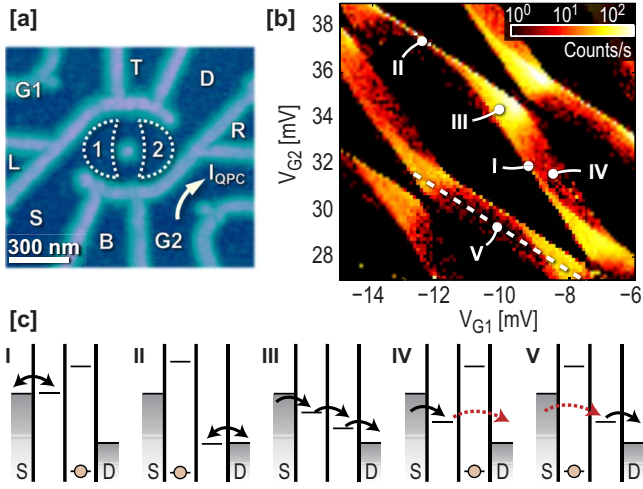
FIG. 1. (Color online) (a) Atomic force microscopy (AFM) image of the sample. The structure consists of a DQD (marked by 1 and 2) with a nearby quantum point contact. (b) Charge stability diagram of the DQD measured by counting electrons entering and leaving the DQD. The data were taken with a voltage bias of $V_{DQD-SD} = 600$ μV applied over the DQD. The QPC conductance was measured with $V_{QPC-SD} = 300$ μV. The count rates were extracted from traces of length $T = 0.5$ s. (c) Energy-level diagrams for different configurations in (b).

out metallic gates so that the coupling between dots and QPC detectors is not screened by metallic structures.

Figure 1(b) shows a charge stability diagram for the DQD measured by counting electrons tunneling into and out of the DQD. The data were taken with a bias voltage of 600 μV applied across the DQD giving rise to finite-bias triangles of sequential transport.[1] The diagrams in Fig. 1(c) show schematics of the DQD energy levels for different positions in the charge stability diagram. Depending on energy-level alignment, different kinds of electron tunneling are possible.

At the position marked by I in Fig. 1(b), the electrochemical potential μ_1 of QD1 is aligned with the Fermi level of the source lead. The tunneling is due to equilibrium fluctuations between the source and QD1. A measurement of the count rate as a function of μ_1 provides a way to determine both the tunneling rate Γ_S and the electron temperature in the source lead.[23] The situation is reversed at point II in Fig. 1(b). Here, electron tunneling occurs between QD2 and the drain, thus, giving an independent measurement of Γ_D and the electron temperature of the drain lead. At point III within the triangle of Fig. 1(b), the levels of both QD1 and QD2 are within the bias window and the tunneling is due to sequential transport of electrons from the source lead into QD1, over to QD2, and finally out to the drain. The electron flow is unidirectional and the count rate relates directly to the current flowing through the system.[17] Between the triangles, there are broad band-shaped regions with low but nonzero count rates where sequential transport is expected to be suppressed due to Coulomb blockade [cases IV and V in Figs. 1(b) and 1(c)]. The finite count rate in this region is attributed to electron tunneling involving virtual processes. These features will be investigated in more detail in Secs. III–VII.

To begin with, we use the time-resolved charge-detection methods to characterize the system. Typical time traces of
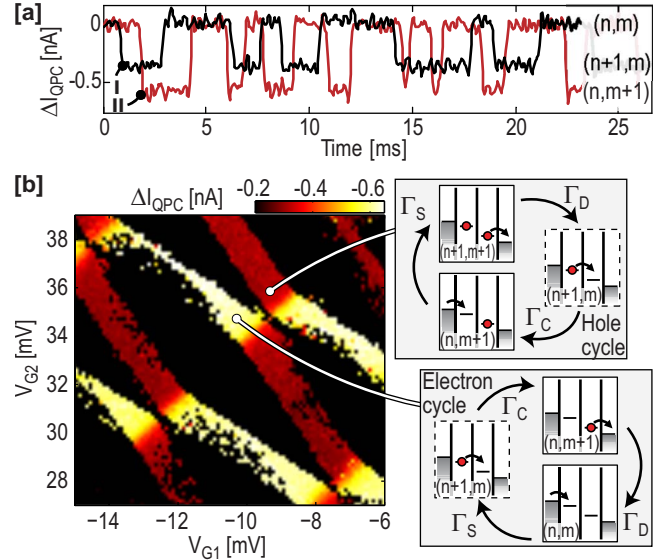

FIG. 2. (Color online) (a) Typical time traces of the QPC current from configurations I and II in Fig. 1(b). (b) Change of QPC current ΔI_{QPC} as one electron enters the DQD, extracted from the same set of data as shown in Fig. 1. The two levels correspond to the QPC detector registering electron tunneling in QD1 and QD2, respectively. The energy-level diagrams describe the hole and the electron cycle of sequential transport within the finite-bias triangles.

the QPC current for DQD configurations marked by I and II in Fig. 1(b) are shown in Fig. 2(a). The QPC current switches between two levels corresponding to electrons entering or leaving QD1 (case I) or QD2 (case II). The change ΔI_{QPC} as one electron enters the DQD is larger for charge fluctuations in QD2 than in QD1. This reflects the stronger coupling between the QPC and QD2 due to the geometry of the device. A measurement of ΔI_{QPC} thus gives information about the charge localization in the DQD.

In Fig. 2(b) we investigate the charge localization in more detail by plotting the absolute change in QPC current ΔI_{QPC} for the same set of data as in Fig. 1(a). The detector essentially only measures two different values of ΔI_{QPC} [either $\Delta I_{QPC} \sim -0.3$ or ~ -0.6 nA]. Comparing the results of Fig. 2(b) with the sketches in Fig. 1(c), we see that regions with high ΔI_{QPC} match with the regions where we expect the counts to be due to electron tunneling in QD2, while the regions with low ΔI_{QPC} come from electron tunneling in QD1.

The regions inside the bias triangles are described in detail in the energy-level diagrams of Fig. 2(b). We assume each QD to hold n and m electrons, respectively. In the lower triangle, the current is carried by a sequential *electron cycle*. Starting from the (n,m) configuration, an electron will tunnel in from the source lead at a rate Γ_S making the transition $(n,m) \rightarrow (n+1,m)$. The electron then passes on to QD2 at a rate $\Gamma_C \sim t/h$ $[(n+1,m) \rightarrow (n,m+1)]$ before leaving to drain at the rate Γ_D $[(n,m+1) \rightarrow (n,m)]$. Since the rate Γ_C is much faster than the detector bandwidth (and $\Gamma_C \gg \Gamma_S$ and $\Gamma_C \gg \Gamma_D$), the detector will only register transitions between the two states (n,m) and $(n,m+1)$. Therefore, we expect the step height ΔI_{QPC} within the lower triangle to be equal to ΔI_{QPC} measured for electron fluctuations in QD2, which is in agreement with the results of Fig. 2.

For the upper triangle, the DQD holds an additional electron and the current is carried by a *hole cycle*. Starting with both QDs occupied $[(n+1,m+1)]$, an electron in QD2 may leave to the drain $[(n+1,m+1)\rightarrow(n+1,m)]$ followed by a fast interdot transition from QD1 to QD2 $[(n+1,m)\rightarrow(n,m+1)]$. Finally, an electron can tunnel into QD1 from the source lead $[(n,m+1)\rightarrow(n+1,m+1)]$. In the hole cycle, the detector is not able to resolve the time the system stays in the $(n+1,m)$ state; the measurement will only register transitions between $(n+1,m+1)$ and $(n,m+1)$. This corresponds to fluctuations of charge in QD1, giving the low value of ΔI_{QPC} in Fig. 2(b). Finally, we note that at the transition between regions of low and high ΔI_{QPC}, the electron wave function delocalizes onto both QDs. This provides a method for determining the interdot coupling energy t.[22] From the data in Fig. 2(b) we find tunnel couplings in the range of 10–50 μeV.

III. COTUNNELING

We now focus on the regions of weak tunneling occurring in regions outside the boundaries expected from sequential transport. In case IV, the electrochemical potential of QD1 is within the bias window, but the potential of QD2 is shifted below the Fermi level of the source and not available for transport. We attribute the nonzero count rate for this configuration to be due to electrons *cotunneling* from QD1 to the drain lead. The time-energy uncertainty principle still allows electrons to tunnel from QD1 to the drain by means of a higher-order process. In case V, the situation is analogous but the roles of the two QDs are reversed; electrons cotunnel from the source into QD2 and leave sequentially to the drain lead.

To investigate the phenomenon more carefully, we measure the rates for electrons tunneling into and out of the DQD in a configuration similar to the configuration along the dashed line in Fig. 1(b). The line corresponds to keeping the electrochemical potential of QD2 fixed within the bias window and sweeping μ_1. The data are presented in Fig. 3. In the region marked by A in Fig. 3, electrons tunnel sequentially from the source into QD1, relax from QD1 down to QD2, and finally tunnel out from QD2 to the drain lead. Proceeding from region A to region B, the electrochemical potential μ_1 is lowered so that an electron eventually gets trapped in QD1. At point B, the electrons lack an energy $\delta_a=\mu_2-\mu_1$ to leave to QD2. Still, electron tunneling is possible by means of a virtual process.[5] Due to the energy-time uncertainty principle, there is a time window of length $\sim\hbar/\delta_a$ within which tunneling from QD1 to QD2 followed by tunneling from the source into QD1 is possible without violating energy conservation. An analogous process is possible involving the next unoccupied state of QD1, occurring on timescales $\sim\hbar/\delta_b$, where $\delta_b=E_{C1}-\delta_a$ and E_{C1} is the charging energy of QD1. The two processes correspond to electron cotunneling from the source lead to QD2. Continuing from points B to C, the unoccupied state of QD2 is shifted into the bias window and electron transport is again sequential.

In the sequential regime (regions A and C), we fit the rate for electrons entering the DQD to a model involving only
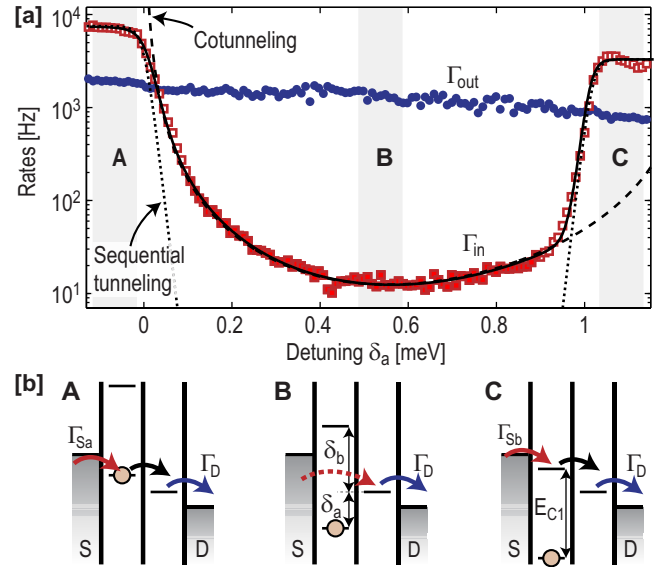

FIG. 3. (Color online) Tunneling rates for electrons entering and leaving the DQD measured while keeping the potential of QD2 fixed and sweeping the electrochemical potential of QD1. The data are measured in a configuration similar to going along the dashed line in Fig. 1(b). The dotted lines are tunneling rates expected from sequential tunneling, while the dashed line is a fit to the cotunneling model of Eq. (1). The solid line corresponds to the model involving molecular states [Eq. (5)]. Parameters are given in text. (b) Schematic of the DQD energy levels for three different configurations in (a). At point A, electrons tunnel sequentially through the structure. Moving to point B, the energy levels of QD1 are shifted and the electron in QD1 is trapped due to Coulomb blockade. Electron transport from the source to QD2 is still possible through virtual processes, but the rate for electrons entering the DQD drops substantially due to the low probability of the virtual processes. At point C, the next level of QD1 is brought inside the bias window and sequential transport is again possible.

sequential tunneling [dotted lines in Fig. 3(a)].[24] The fit allows us to determine the tunnel couplings between the source and the occupied (Γ_{Sa})/unoccupied (Γ_{Sb}) states of QD2, giving $\Gamma_{Sa}=7.5$ kHz, $\Gamma_{Sb}=3.3$ kHz, and $T=100$ mK. Going toward region B, the rates due to sequential tunneling are expected to drop exponentially as the energy difference between the levels in QD1 and QD2 is increased. In the measurement, the rate Γ_{in} initially decreases with detuning, but the decrease is slower than exponential and flattens out as the detuning gets larger. This is in strong disagreement with the behavior expected for sequential tunneling. Instead, in a region around point B we attribute the measured rate Γ_{in} to be due to electrons cotunneling from the source to QD2.

The rate for cotunneling from the source to QD2 is given as[25]

$$\Gamma_{cot} = \Gamma_{Sa}\frac{t_a^2}{\delta_a^2} + \Gamma_{Sb}\frac{t_b^2}{\delta_b^2} + \cos\phi\sqrt{\Gamma_{Sa}\Gamma_{Sb}}\frac{t_a t_b}{\delta_a \delta_b}. \quad (1)$$

Here, t_a and t_b are the tunnel couplings between the occupied or unoccupied states in QD1 and the state in QD2. The first term describes cotunneling involving the occupied state of QD1, the second term describes the cotunneling over the

unoccupied state, and the third term accounts for possible interference between the two. The phase ϕ defines the phase difference between the two processes. To determine ϕ one needs to be able to tune the phases experimentally, which is not possible from the measurement shown in Fig. 3(a). In the following we therefore assume the two processes to be independent ($\phi = \pi/2$). Interference effects between cotunneling processes have been studied in detail in Ref. 15.

The dashed line in Fig. 3(a) shows the results of Eq. (1) with fitting parameters $t_a = 15$ μeV and $t_b = 33$ μeV. These values are in good agreement with values obtained from charge localization measurements. The values for Γ_{Sa} and Γ_{Sb} are taken from measurements in the sequential regimes. We emphasize that Eq. (1) is valid only if $\delta_a, \delta_b \gg t_a, t_b$ and if sequential transport is sufficiently suppressed. The data points used in the fitting procedure are marked by filled squares in the figure. It should be noted that the sequential tunneling in region C prevents investigation of the cotunneling rate at small δ_b. This can easily be overcome by inverting the DQD bias. The rate for electrons tunneling out of the DQD [Γ_{out} in Fig. 3(a)] shows only slight variations over the region of interest. This is expected since μ_2 stays constant over the sweep. The slight decay of Γ_{out} with increased detuning comes from tuning the tunnel barrier between QD2 and the drain.[26]

The cotunneling may be modified by the existence of a nearby QPC. If the QPCs were able to detect the presence of electron in QD2 during the cotunneling, we would expect this to influence the cotunneling process. For the measurements in Fig. 3(a) the QPC current was kept below 10 nA. This gives an average time delay between two electrons passing the QPC of $e/I_{QPC} \sim 16$ ps. Since this is larger than the typical cotunneling time, it is unlikely that the electrons in the QPC are capable of detecting the cotunneling process. The influence of the QPC may become important for larger QPC currents. However, when the QPC bias voltage is larger than the detuning ($eV_{QPC} > \delta$), the fluctuations in the QPC current may start to drive inelastic charge transitions between the QDs.[15,20] Such transitions will compete with the cotunneling. For this reason it was not possible to extract what effect the presence of the QPC may have on the cotunneling process.

IV. MOLECULAR STATES

The overall good agreement between Eq. (1) and the measured data demonstrates that time-resolved charge-detection techniques provide a direct way of quantitatively using the time-energy uncertainty principle. However, a difficulty arises as $\delta \rightarrow 0$; the cotunneling rate in Eq. (1) diverges as visualized for the dashed line in Fig. 3(a). The problem with Eq. (1) is that it only takes second-order tunneling processes into account. For small detuning δ the cotunneling described in Eq. (1) must be extended to include higher-order processes.[27]

A different approach is to assume the coupling between the QDs to be fully coherent and describe the DQD in terms of the bonding and antibonding molecular states.[28,29] Both the sequential tunneling and the cotunneling can then be

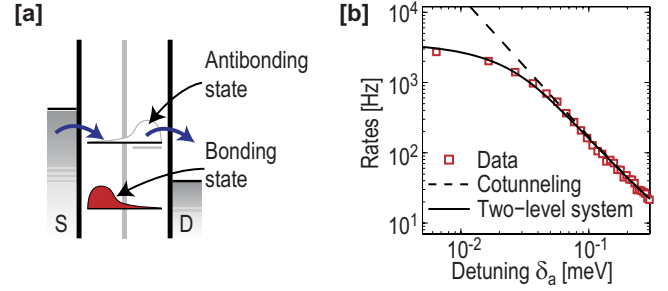**[a]** Antibonding state / Bonding state / S / D

[b]

FIG. 4. (Color online) (a) Cotunneling described using molecular states. Due to the large detuning the empty antibonding state is mainly localized on QD2, but a small part of the wave function is still present in QD1 which allows an electron to enter from the source. (b) The rate for electrons tunneling into the DQD (Γ_{in}) as a function of DQD detuning δ_a. The figure shows the same data as in Fig. 3 but plotted on a log-log scale to enhance the features at small detuning. The dashed line is the result of the cotunneling model in Eq. (1) and the solid line shows the result of the molecular-state model [Eq. (5)].

treated as first-order tunneling processes into the molecular states; what we referred to in Fig. 3 as cotunneling would be tunneling into an antibonding state. The model is sketched in Fig. 4(a). The bonding state is occupied and in Coulomb blockade. Still, an electron may tunnel from the drain into the antibonding state. Due to the large detuning, the antibonding state is mainly located on QD2, the overlap with the electrons in the source lead is small, and the tunneling is weak. Changing the detuning will have the effect of changing the shape of the molecular states and shift their weights between the two QDs.

To calculate the rate for electron tunneling from the source into the molecular state of the DQD as visualized in Fig. 4(a), we consider the DQD as a tunnel-coupled two-level system containing one electron, which is isolated from the environment. We introduce the basis states $\{\Psi_1, \Psi_2\}$ describing the electron sitting on the left or right QD, respectively. The two states are tunnel coupled with coupling t and separated in energy by the detuning δ. The Hamiltonian of the system is

$$H = \begin{bmatrix} -\delta/2 & t \\ t & \delta/2 \end{bmatrix}. \quad (2)$$

The eigenvectors of the Hamiltonian in Eq. (2) form the bonding Ψ_B and antibonding states Ψ_A of the system. The eigenvalues give the energies E_B and E_A of the two states with

$$E_B = -\frac{1}{2}\sqrt{4t^2 + \delta^2}, \quad E_A = \frac{1}{2}\sqrt{4t^2 + \delta^2}. \quad (3)$$

Note that at zero detuning there is still a finite level separation set by the tunnel coupling. The occupation probabilities p_B and p_A of the two states are determined by detailed balance,

$$p_B = 1 - \frac{1}{1 + e^{\sqrt{4t^2 + \delta^2}/k_B T}}, \quad p_A = \frac{1}{1 + e^{\sqrt{4t^2+\delta^2}/k_B T}}. \quad (4)$$

To calculate the rate for electrons tunneling from the source into the antibonding molecular state of the DQD as visualized in Fig. 4(a), we project the thermal population p_B and p_A of the molecular states Ψ_B and Ψ_A onto the unperturbed state of QD1, Ψ_1. This gives the probability p_1 of finding an electron in QD1 if making a projective measurement in the Ψ_1 basis. The measured rate Γ_{in} is equal to the probability of finding QD1 being empty $(1-p_1)$ multiplied with Γ_S, which is the tunneling rate between the source and the unperturbed state in QD1,

$$\Gamma_{in} = \Gamma_S(1 - p_1) = \Gamma_S[1 - (p_B\Psi_B + p_A\Psi_A) \cdot \Psi_1]$$
$$= \Gamma_S \frac{1}{2}\left(1 - \frac{\delta \tanh(\sqrt{4t^2 + \delta^2}/2k_B T)}{\sqrt{4t^2 + \delta^2}}\right). \quad (5)$$

For large detuning, the bonding and antibonding states are well localized in QD1 and QD2, respectively. Here, we should recover the results for the cotunneling rate obtained for the second-order process [Eq. (1)]. First, we assume low temperature $k_B T \ll \delta$ so that the electron only populates the bonding ground state ($p_B = 1$ and $p_A = 0$),

$$\Gamma_{in} = \Gamma_S \frac{1}{2}\left(1 + \frac{\delta}{\sqrt{4t^2 + \delta^2}}\right). \quad (6)$$

In the limit $\delta \gg t$ the relation reduces to $\Gamma_{in} \approx \Gamma_S t^2/\delta^2$ and the rate approaches the result of the second-order cotunneling processes in Eq. (1). The advantage of the molecular-state model is that it is valid for any detuning both in the sequential and in the cotunneling regimes.

The solid line in Fig. 3(a) shows the results of Eq. (5). The equation has been evaluated twice—once for the occupied $[(n,m)]$ state and once for the unoccupied state in QD2 $[(n,m+1)]$; the curve in Fig. 3(a) is the sum of the two rates. The same parameters were used for the cotunneling fit of Eq. (1). The model shows very good agreement with data over the full range of the measurement. To compare the results of the molecular-state and the cotunneling models in the regime of small detuning, we plot the data in Fig. 3(a) on a log-log scale [Fig. 4(b)]. For large detuning, the tunneling rate follows the $1/\delta^2$ predicted by both the molecular-state and the cotunneling models. For small detuning, the deviations become apparent as the cotunneling model diverges, whereas the molecular-state model still reproduces the data well.

V. EXCITED STATES

So far, we have only considered cotunneling involving the ground states of the two QDs. The situation is more complex if we include excited states in the model; the measured rate may come from a combination of cotunneling processes involving different QD states. To investigate the influence of excited states experimentally, we start by extracting the DQD excitation spectrum using finite-bias spectroscopy.[1] If the coupling between the QDs is weak ($t_C \ll \Delta E_1$ and ΔE_2 with $\Delta E_{1,2}$ being the mean level spacing in each QD), the DQD
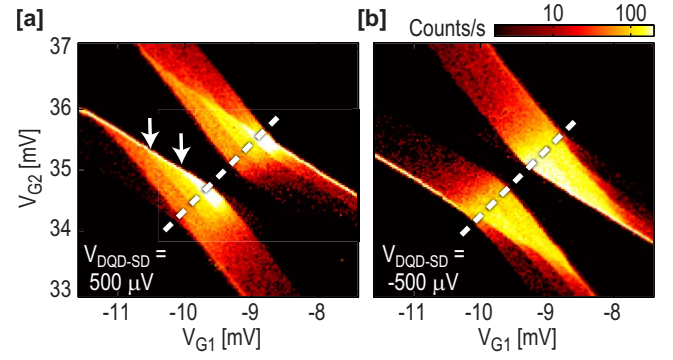

FIG. 5. (Color online) Finite-bias spectroscopy of the DQD taken with (a) positive and (b) negative biases. The figures are constructed by counting electrons entering and leaving the DQD. Excited states are visible, especially for the positive bias data [marked with arrows in (a)]. The data were taken with $V_{DQD-SD} = \pm 500$ μV and $V_{QPC-SD} = 250$ μV.

spectrum essentially consists of the combined excitation spectrum of the individual QDs. For a more strongly coupled DQD the QD states residing in different dots will hybridize and delocalize over both QDs. In this section we consider a relatively weakly coupled configuration ($t \sim 25$ μeV) and assume the excited states to be predominantly located within the individual QDs.

Figure 5 shows a magnification of two triangles from Fig. 1(b) measured with both negative and positive biases applied across the DQD. Excited states are visible within the triangles, especially for the case of positive bias [marked with arrows in Fig. 5(a)]. Transitions between excited states occur along parallel lines at which the potential of QD1 is held constant; this indicates that the excited states are located in QD1. To investigate the states more carefully, we measure the separate tunneling rates Γ_{in} and Γ_{out} along the dashed lines in Fig. 5. The results are presented in Fig. 6 together with a few sketches depicting the energy-level configuration of the system.

We begin with the results for the positive bias case, which are plotted in Fig. 6(a). Going along the dashed line in Fig. 5(a) corresponds to keeping the detuning δ between the fixed QDs and shifting the total DQD energy. The measurements were performed with a small detuning ($\delta \approx 100$ μeV) to ensure that the electron transport is unidirectional. Because of this, the outermost parts of the traces in Fig. 6(a) correspond to regions where transport is due to cotunneling [compare the dashed line with the position of the triangle in Fig. 5(a)]; the regions where transport is sequential are shaded gray in Fig. 6(a).

Starting in the regime marked by I in Figs. 6(a) and 6(c), electrons may tunnel from the source into the ground state of QD1, relax down to QD2, and tunnel out to the drain lead. Assuming the relaxation process to be much faster than the other processes, the measured rates Γ_{in} and Γ_{out} are related to the tunnel couplings of the source and drain ($\Gamma_{in} \approx \Gamma_S$ and $\Gamma_{out} = \Gamma_D$). Going to higher gate voltages lowers the overall energy of both QDs. At the position marked by an arrow in Fig. 6(a), there is a sharp increase in the rate for tunneling into the DQD. We attribute this to the existence of an excited
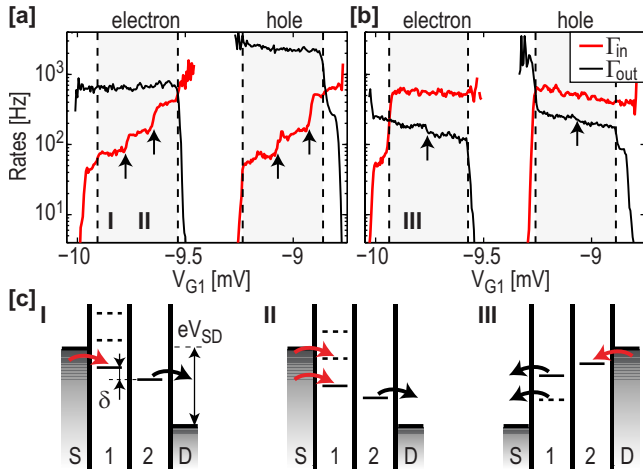
FIG. 6. (Color online) [(a) and (b)] Tunneling rates for electrons entering and leaving the DQD measured along the dashed lines in Figs. 5(a) and 5(b). In (a), we show the results for positive bias across the DQD and in (b) the results for negative bias. The shaded areas mark the regions where electron transport is sequential either in the electron or the hole transport cycle. The arrows indicate the positions of excited states. The data were extracted from QPC conductance traces of length $T=5$ s taken with $V_{QPC-SD}=250$ mV. (c) Schematics of the DQD energy configuration at three different positions in (a) and (b).

state in QD1; as shown in case II in Fig. 6(c), the electron tunneling from the source into QD1 may enter either into the ground $(n+1,m)$ or the excited state $(n+1^*,m)$ giving an increase in Γ_{in}. When further lowering the DQD energy another excited state comes into the bias window and Γ_{in} increases even more [second arrow in Fig. 6(a)]. The rate for tunneling out of the DQD shows only minor variations within the region of interest. This supports the assumption that the excited states quickly relax and that the electron tunnels out of the DQD from the ground state of QD2.

Finally, continuing to the edge of the shaded region $(V_{G1} \sim -9.55$ mV$)$, the potential of QD2 goes below the Fermi level of the drain. Here, electrons get trapped in QD2 and the tunneling-out rate drops drastically. At the same time, Γ_{in} increases; when the electron in QD2 eventually tunnels out, the DQD may be refilled from either the source or the drain lead. The picture described above is repeated in the triangle with hole transport $(-9.25$ mV$<V_{G2}<-8.9$ mV$)$. This is expected, since the hole transport cycle involves the same QD states as in the electron case. An interesting feature is that Γ_{in} shows essentially the same values in both the electron and the hole cycles, while Γ_{out} increases by a factor of three. The presence of the additional electron in QD1 apparently affects the tunnel barrier between the drain and QD2 more than an additional electron in QD2 affects the barrier between QD1 and the source.

Next, we move over to the case of negative bias [Fig. 6(b)]. Here, the roles of QD1 and QD2 are inverted, which means that electrons enter the DQD into QD2 and leave from QD1. Following the data and the arguments presented for the case of positive bias, one would expect this configuration to be suitable for detecting excited states in QD2. However, looking at the tunneling rates within the sequential region of

Fig. 6(b), the rate for entering QD2 (Γ_{in}) stays fairly constant, while the rate for tunneling out decreases at the point marked by the arrow. Again, we attribute the behavior to the existence of an excited state in QD1.

The situation is described in sketch III of Fig. 6(c). The electrochemical potential of QD1 is high enough to allow the electron in the $(n+1,m)$ state to tunnel out to the source and leave the DQD in an excited state (n^*,m). Since the energy difference $E[(n^*,m)]-E[(n+1,m)]$ is smaller than $E[(n,m)]-E[(n+1,m)]$, the transition involving the excited state appears *below* the ground-state transition. As the overall DQD potential is lowered, the transition energy involving the excited state goes below the Fermi level of the drain, resulting in a drop of Γ_{out} as only the ground-state transition is left available. Similar to the single QD case,[23] the tunneling-in rate samples the excitation spectrum for the $(n+1,m)$ configuration, while the tunneling-out rate reflects the excitation spectrum of the (n,m) DQD.

To conclude the results of Fig. 6, we find two excited states in QD1 in the $(n+1,m)$ configuration with $\Delta E_1^\alpha = 180$ μeV and $\Delta E_1^\beta = 340$ μeV, and one excited state in QD1 in the (n,m) configuration with $\Delta E_1 = 220$ μeV. No clear excited state is visible in QD2. This does not necessarily mean that such states do not exist; if they are weakly coupled to the lead they will only have a minor influence on the measured tunneling rates. Excited states in both QDs have been measured in other configurations; there, we find similar spectra of excited states for both QDs.

VI. INELASTIC COTUNNELING

Next, we investigate the cotunneling process in the presence of excited states. Looking carefully at the lower-right regions of the negative-bias triangles in Fig. 5(b), we see that the count rates in the cotunneling regions outside the triangles are not constant along lines of fixed detuning (corresponds to going in a direction parallel to the dashed line). Instead, the cotunneling regions seem to split into three parallel bands.

In Fig. 7(a), we plot the tunneling rates Γ_{in} and Γ_{out} for electrons entering and leaving the DQD extracted from the same set of data as used in Fig. 5(b). The thick solid lines mark the edges of the finite-bias triangles. Again, the cotunneling rates outside the triangles are not uniform; parallel bands appear in Γ_{in} for the position marked by I and in Γ_{out} for the position marked by II in the figures.

To understand the data we draw energy-level diagrams for the two configurations [see Fig. 7(b)]. Focusing first on case I, we see that the electrochemical potential of QD1 is within the bias window, whereas QD2 is detuned and in Coulomb blockade. The cotunneling occurs via QD2 states; electrons cotunnel from the drain into QD1 followed by sequential tunneling from QD1 to the source lead. The picture is in agreement with what is measured in Fig. 7(a); the cotunneling rate (Γ_{in}) is low and strongly depends on detuning δ, while the sequential rate Γ_{out} is high and essentially independent of detuning. The three bands seen in Γ_{in} occur because of the excited states in QD1; depending on the average DQD energy, electrons may cotunnel from the drain into one of the
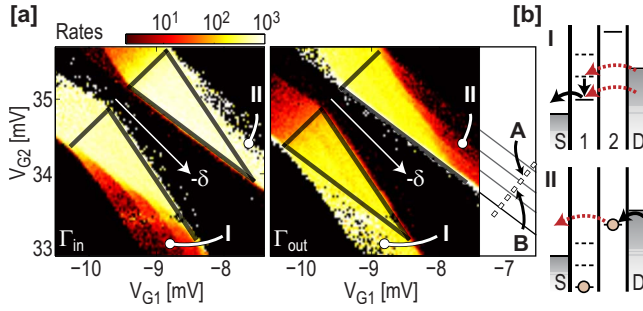
FIG. 7. (Color online) (a) Tunneling rates for electrons entering and leaving the DQD extracted from the same set of data as used in Fig. 5(b). The data were measured with $V_{\text{DQD-SD}}=-500$ μV. The solid lines mark the position of the finite-bias triangles. The plot region in the right-hand panel has been extended to include the regime investigated in Fig. 8. (b) Energy-level diagrams for the two positions marked in (a). In case I, the cotunneling itself is elastic with energy relaxation occurring after the cotunneling has taken place. In case II, inelastic cotunneling processes are possible.

excited states, relax to the ground state, and then leave to the source lead. The state of QD2 remains unaffected by the cotunneling process. For this configuration, we speak of *elastic* cotunneling.

The situation is different in case II. Here, cotunneling occurs in QD1 as electrons tunnel directly from QD2 into the source lead. This means that Γ_{in} is sequential while Γ_{out} describes the cotunneling process. As in case I, the cotunneling rate Γ_{out} splits up into three bands; we attribute this to cotunneling where the state of QD1 is changed during the process. QD1 ends up in one of its excited states. The energy of the electron arriving in the source lead is correspondingly decreased compared to the electrochemical potential of QD2. Here, the cotunneling is *inelastic*.

The inelastic cotunneling is described in greater detail in Fig. 8. In Fig. 8(a) we plot the count rate for positive and negative DQD biases measured along the dashed line at the right edge of Fig. 7(a). Figure 8(b) shows energy-level diagrams for negative bias at two positions along this line. The bias voltage is applied symmetrically to the DQD, which means that the Fermi levels in the source and drain leads are shifted by $\pm eV/2$ relative to the Fermi energy at zero bias [dotted line in Fig. 8(b)]. In the measurement of Fig. 8(a) we sweep the average DQD energy while keeping the detuning δ constant. The average DQD energy is defined to be zero when μ_2 aligns with the zero-bias Fermi energy in the leads [i.e., when $\mu_2=(\mu_S+\mu_D)/2$].

Starting in the configuration marked by A, cotunneling is only possible involving the QD2 ground state. Cotunneling is weak with count rates being well below 1 count/s. Continuing to case B, we raise the average DQD energy. When the electrochemical potential of QD2 is sufficiently increased compared to the Fermi level of the source, inelastic cotunneling becomes possible leading to a sharp increase in count rate. The process is sketched in Fig. 8(b); it involves the simultaneous tunneling of an electron from QD2 to the first excited state of QD1 with an electron in the QD1 ground state leaving to the source. The process is only possible if
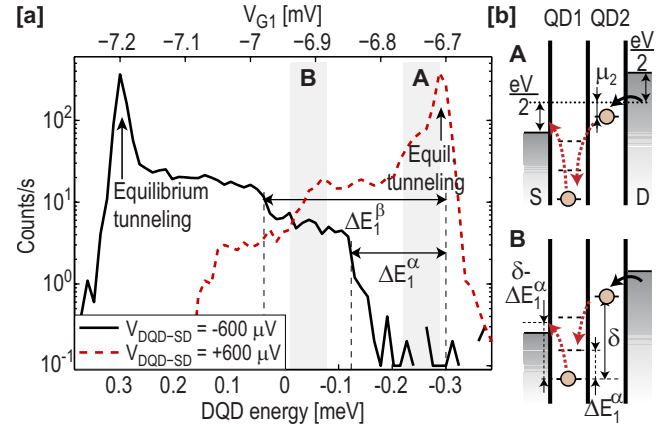

FIG. 8. (Color online) (a) Electron count rate along the dashed line in Fig. 7(a) measured for both positive and negative DQD biases. In the trace, the detuning δ stays constant and we sweep the average DQD energy. The DQD energy is defined from the position where the electrochemical potential of QD2 is right in the middle between the Fermi levels of the source and drain leads [see the dotted line in the energy-level diagram in (b)]. The steps in the count rate are due to the onset of inelastic cotunneling processes in QD1. The data were extracted from traces of length $T=10$ s measured with $V_{\text{QPC-SD}}=200$ μV. (b) Energy-level diagrams for the two configurations marked in (a).

$$\delta - \Delta E_1^\alpha = \mu_1 - \mu_2 - \Delta E_1^\alpha > \mu_S - \mu_1. \qquad (7)$$

Here, ΔE_1^α is the energy of the first excited state in QD1. The position of the step in Fig. 8(a) directly gives the energy of the first excited state, and we find $\Delta E_1^\alpha=180$ μeV.

Further increasing the average DQD energy makes an inelastic process involving the second excited state in QD2 possible, giving $\Delta E_2^\alpha=340$ μeV. Finally, as the DQD energy is raised to become equal to half the applied bias, the electrochemical potential of QD2 aligns with Fermi level of the drain lead. Here electron tunneling mainly occurs due to equilibrium fluctuations between the drain and QD2, giving a sharp peak in the count rate. The excited-state energies extracted from the inelastic cotunneling give the same values as obtained from finite-bias spectroscopy within the triangles as described in Sec. V. The good agreement between the two measurements demonstrates the consistency of the model.

The dashed line in Fig. 8(a) shows data taken with reversed DQD bias; for this configuration the Fermi levels of the source and drain leads are inverted, the electrons cotunnel from the source to QD2, and the peak due to equilibrium tunneling occurs at $\mu_2=\mu_D=-300$ μeV.

VII. NOISE IN THE COTUNNELING REGIME

Using time-resolved charge-detection methods, we can extract the noise of electron transport in the cotunneling regime. For a weakly coupled single QD in the regime of sequential tunneling, transport in most configurations is well described by independent tunneling events for electrons entering and leaving the QD.[16] The Fano factor becomes a function of the tunneling rates,[30]
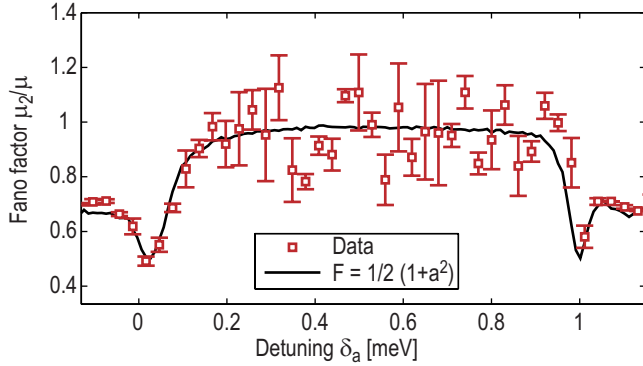
FIG. 9. (Color online) Fano factor for electron transport in the cotunneling regime of Fig. 3. The data were extracted from traces of length $T=30$ s. The solid line is the result of Eq. (8), which assumes independent tunneling events. The minima in Fano factor occur at positions where the tunneling rates Γ_{in} and Γ_{out} are equal (see Fig. 3). The error bars show standard error extracted by splitting the data into six subsets of length $T=5$ s and evaluating the noise for each subset.

$$F_2 = \frac{S_I}{2eI} = \frac{\Gamma_{in}^2 + \Gamma_{out}^2}{(\Gamma_{in} + \Gamma_{out})^2} = \frac{1}{2}(1 + a^2), \qquad (8)$$

with $a=(\Gamma_{in}-\Gamma_{out})/(\Gamma_{in}+\Gamma_{out})$. For symmetric barriers ($a=0$), the Fano factor is reduced to 0.5 because of an increase in electron correlation due to Coulomb blockade. In the case of cotunneling, the situation is more complex. As described in Sec. VI, cotunneling may involve processes leaving QD in an excited state. The excited state has a finite lifetime τ_{rel}; during this time, the tunneling rates may be different compared to the ground-state configuration.[8] We therefore expect that the existence of an electron in an excited state may induce temporal correlations on time scales on the order of τ_{rel} between subsequent cotunneling events. In this way, the noise of the cotunneling current has been proposed as a tool to probe excited states and relaxation processes in QDs.[31,32]

In Fig. 9, we plot the Fano factor measured from the same region as that of Fig. 3. The Fano factor was extracted by measuring the distribution function for transmitted charge through the system.[16] The solid line shows the result of Eq. (8) with tunneling rates extracted from the measured traces. In the outermost regions of the graph, the electrons tunnel sequentially through the DQD. Here, the Fano factor is reduced due to Coulomb blockade similar to the single QD

case. At the edges of the cotunneling regions, the Fano factor drops further down to $F=0.5$. This is because the injection rate Γ_{in} drops drastically as sequential transport becomes unavailable, while Γ_{out} stays approximately constant. At some point we get $\Gamma_{in}=\Gamma_{out}$, which means that the asymmetry a is zero and the Fano factor of Eq. (8) shows a minimum. Further into the cotunneling region, the Fano factor approaches one as transport essentially becomes limited by a single rate; the cotunneling rate (Γ_{in}) is two orders of magnitude smaller than the sequential rate Γ_{out}.

We do not see any major deviation from the results of Eq. (8), which is only valid assuming independent tunneling events. We have performed similar measurements in several inelastic and elastic cotunneling regimes without detecting any clear deviations from Eq. (8). As it turns out, there are two effects that make it hard to detect correlations due to the internal QD relaxations. For the first, the correlation time is essentially set by the relaxation time τ_{rel}, which typically occurs on a ~ 10 ns timescale. This is several orders of magnitude smaller than a typical tunneling time of $\sim 1/\Gamma_{in}$ ~ 100 ms.[33] Second, the slow cotunneling rate limits the amount of experimental data available within a reasonable measurement time. This explains the large spread between the data points in Fig. 9 in the cotunneling regime. We conclude that the measurement bandwidth currently limits the possibility of examining correlations in the cotunneling regime using time-resolved detection techniques. A higher-bandwidth detector would solve both the above mentioned problems. It would allow a general increase in the tunneling rates in the system, which would both decrease the difference between τ_{cot} and τ_{rel} as well as provide faster acquisition of sufficient statistics.

To conclude, we have used time-resolved charge-detection techniques to investigate tunneling of single electrons involving virtual processes. The measurement method provides precise determination of all coupling energies, which allows a direct comparison with tunneling rates expected from time-energy uncertainty. The results give experimental confirmation of the equivalence between cotunneling through atomic states and sequential tunneling into molecular states. In the high-bias regime, we measure inelastic cotunneling due to virtual processes involving excited states of the double quantum dot. For future experiments with a high-bandwidth detector, the method may provide a way to probe relaxation processes and internal charge dynamics in quantum dots.

*simongus@phys.ethz.ch

[1] W. G. van der Wiel, S. De Franceschi, J. M. Elzerman, T. Fujisawa, S. Tarucha, and L. P. Kouwenhoven, Rev. Mod. Phys. **75**, 1 (2002).

[2] T. Hayashi, T. Fujisawa, H. D. Cheong, Y. H. Jeong, and Y. Hirayama, Phys. Rev. Lett. **91**, 226804 (2003).

[3] J. R. Petta, A. C. Johnson, C. M. Marcus, M. P. Hanson, and A. C. Gossard, Phys. Rev. Lett. **93**, 186802 (2004).

[4] V. N. Golovach and D. Loss, Phys. Rev. B **69**, 245327 (2004).

[5] D. V. Averin and Y. V. Nazarov, Phys. Rev. Lett. **65**, 2446 (1990).

[6] S. De Franceschi, S. Sasaki, J. M. Elzerman, W. G. van der Wiel, S. Tarucha, and L. P. Kouwenhoven, Phys. Rev. Lett. **86**, 878 (2001).

[7] D. M. Zumbühl, C. M. Marcus, M. P. Hanson, and A. C. Gossard, Phys. Rev. Lett. **93**, 256801 (2004).

[8] R. Schleser, T. Ihn, E. Ruh, K. Ensslin, M. Tews, D. Pfannkuche, D. C. Driscoll, and A. C. Gossard, Phys. Rev. Lett. **94**, 206805 (2005).

[9] H. W. Liu, T. Fujisawa, T. Hayashi, and Y. Hirayama, Phys. Rev. B **72**, 161305(R) (2005).

[10] M. Field, C. G. Smith, M. Pepper, D. A. Ritchie, J. E. F. Frost, G. A. C. Jones, and D. G. Hasko, Phys. Rev. Lett. **70**, 1311 (1993).

[11] T. Fujisawa, T. Hayashi, Y. Hirayama, H. D. Cheong, and Y. H. Jeong, Appl. Phys. Lett. **84**, 2343 (2004).

[12] R. Schleser, E. Ruh, T. Ihn, K. Ensslin, D. C. Driscoll, and A. C. Gossard, Appl. Phys. Lett. **85**, 2005 (2004).

[13] L. M. K. Vandersypen, J. M. Elzerman, R. N. Schouten, L. H. Willems van Beveren, R. Hanson, and L. P. Kouwenhoven, Appl. Phys. Lett. **85**, 4394 (2004).

[14] J. M. Elzerman, R. Hanson, L. H. Willems van Beveren, B. Witkamp, L. M. K. Vandersypen, and L. P. Kouwenhoven, Nature (London) **430**, 431 (2004).

[15] S. Gustavsson, R. Leturcq, M. Studer, T. Ihn, K. Ensslin, D. C. Driscoll, and A. C. Gossard, Nano Lett. **8**, 2547 (2008).

[16] S. Gustavsson, R. Leturcq, B. Simovic, R. Schleser, T. Ihn, P. Studerus, K. Ensslin, D. C. Driscoll, and A. C. Gossard, Phys. Rev. Lett. **96**, 076605 (2006).

[17] T. Fujisawa, T. Hayashi, R. Tomita, and Y. Hirayama, Science **312**, 1634 (2006).

[18] S. Gustavsson, I. Shorubalko, R. Leturcq, S. Schön, and K. Ensslin, Appl. Phys. Lett. **92**, 152101 (2008).

[19] A. Fuhrer, A. Dorn, S. Lüscher, T. Heinzel, K. Ensslin, W. Wegscheider, and M. Bichler, Superlattices Microstruct. **31**, 19 (2002).

[20] S. Gustavsson, M. Studer, R. Leturcq, T. Ihn, K. Ensslin, D. C. Driscoll, and A. C. Gossard, Phys. Rev. Lett. **99**, 206804 (2007).

[21] O. Naaman and J. Aumentado, Phys. Rev. Lett. **96**, 100201 (2006).

[22] L. DiCarlo, H. J. Lynch, A. C. Johnson, L. I. Childress, K. Crockett, C. M. Marcus, M. P. Hanson, and A. C. Gossard, Phys. Rev. Lett. **92**, 226801 (2004).

[23] S. Gustavsson, R. Leturcq, B. Simovic, R. Schleser, P. Studerus, T. Ihn, K. Ensslin, D. C. Driscoll, and A. C. Gossard, Phys. Rev. B **74**, 195305 (2006).

[24] L. P. Kouwenhoven, C. M. Marcus, P. M. McEuen, S. Tarucha, R. M. Westervelt, and N. S. Wingreen, in *Mesoscopic Electron Transport*, NATO Advanced Studies Institute, Series E: Applied Science No. 345, edited by L. L. Sohn, L. P. Kouwenhoven, and G. Schön (Kluwer, Dordrecht, 1997), pp. 105–214.

[25] D. V. Averin and Y. V. Nazarov, *Single Charge Tunneling* (Plenum, New York, 1992).

[26] K. MacLean, S. Amasha, I. P. Radu, D. M. Zumbühl, M. A. Kastner, M. P. Hanson, and A. C. Gossard, Phys. Rev. Lett. **98**, 036802 (2007).

[27] T. Pohjola, J. Konig, M. M. Salomaa, J. Schmid, H. Schoeller, and G. Schon, Europhys. Lett. **40**, 189 (1997).

[28] M. R. Gräber, W. A. Coish, C. Hoffmann, M. Weiss, J. Furer, S. Oberholzer, D. Loss, and C. Schönenberger, Phys. Rev. B **74**, 075427 (2006).

[29] J. N. Pedersen, B. Lassen, A. Wacker, and M. H. Hettler, Phys. Rev. B **75**, 235314 (2007).

[30] J. H. Davies, P. Hyldgaard, S. Hershfield, and J. W. Wilkins, Phys. Rev. B **46**, 9620 (1992).

[31] J. Aghassi, A. Thielmann, M. H. Hettler, and G. Schön, Phys. Rev. B **73**, 195323 (2006).

[32] J. Aghassi, M. H. Hettler, and G. Schon, Appl. Phys. Lett. **92**, 202101 (2008).

[33] T. Fujisawa, D. G. Austing, Y. Tokura, Y. Hirayama, and S. Tarucha, Nature (London) **419**, 278 (2002).